frontiers in Chemistry

ORIGINAL RESEARCH
published: 15 April 2021
doi: 10.3389/fchem.2021.670612

Promoting the Performance of Li–CO_2 Batteries via Constructing Three-Dimensional Interconnected K^+ Doped MnO_2 Nanowires Networks

*Zhuolin Tang[1], Mengming Yuan[1], Huali Zhu[2], Guang Zeng[1], Jun Liu[1], Junfei Duan[1] and Zhaoyong Chen[1]**

[1] College of Materials Science and Engineering, Changsha University of Science and Technology, Changsha, China, [2] School of Physics and Electronic Science, Changsha University of Science and Technology, Changsha, China

OPEN ACCESS

Edited by:
Wei Xiao,
Yangtze University, China

Reviewed by:
Xing Li,
Southwest Petroleum University, China
Bin Wang,
China Academy of Engineering Physics, China
Xunhui Xiong,
South China University of Technology, China

***Correspondence:**
Zhaoyong Chen
chenzhaoyongcioc@126.com

Specialty section:
This article was submitted to Electrochemistry, a section of the journal Frontiers in Chemistry

Received: *22 February 2021*
Accepted: *22 March 2021*
Published: *15 April 2021*

Citation:
Tang Z, Yuan M, Zhu H, Zeng G, Liu J, Duan J and Chen Z (2021) Promoting the Performance of Li–CO_2 Batteries via Constructing Three-Dimensional Interconnected K^+ Doped MnO_2 Nanowires Networks. Front. Chem. 9:670612. doi: 10.3389/fchem.2021.670612

Nowadays, Li–CO_2 batteries have attracted enormous interests due to their high energy density for integrated energy storage and conversion devices, superiorities of capturing and converting CO_2. Nevertheless, the actual application of Li–CO_2 batteries is hindered attributed to excessive overpotential and poor lifespan. In the past decades, catalysts have been employed in the Li–CO_2 batteries and been demonstrated to reduce the decomposition potential of the as-formed Li_2CO_3 during charge process with high efficiency. However, as a representative of promising catalysts, the high costs of noble metals limit the further development, which gives rise to the exploration of catalysts with high efficiency and low cost. In this work, we prepared a K^+ doped MnO_2 nanowires networks with three-dimensional interconnections (3D KMO NWs) catalyst through a simple hydrothermal method. The interconnected 3D nanowires network catalysts could accelerate the Li ions diffusion, CO_2 transfer and the decomposition of discharge products Li_2CO_3. It is found that high content of K^+ doping can promote the diffusion of ions, electrons and CO_2 in the MnO_2 air cathode, and promote the octahedral effect of MnO_6, stabilize the structure of MnO_2 hosts, and improve the catalytic activity of CO_2. Therefore, it shows a high total discharge capacity of 9,043 mAh g^{-1}, a low overpotential of 1.25 V, and a longer cycle performance.

Keywords: Li-CO_2 batteries, K^+ doped MnO_2 nanowires, interconnect networks, CO_2 conversion, low overpotential

INTRODUCTION

The excessive use of fossil resources makes the earth's carbon dioxide (CO_2) flux unable to reach an effective balance, which has a huge impact on global warming, human health (Chu and Majumdar, 2012; Sanz-Perez et al., 2016). In recent years, continuous studies have been devoted to develop advanced CO_2 capture and storage technologies for the reduction of CO_2 emissions (Nguyen and Dinh, 2020). Among them, direct electrochemical reduction of CO_2 with electron transfer is an effective solution for the capture and conversion of CO_2 into sustainable energy (Khurram et al., 2018). Compared to other CO_2 conversion techniques such as algae-based biofuel

production (De Bhowmick et al., 2019), carbonate fixation (Jang et al., 2016), electrochemical conversion and energy storage devices (Appel et al., 2013), Li-CO_2 battery has a higher discharge potential and specific energy density, so it is considered to be one of the most promising candidates (Xie et al., 2017).

In Li–CO_2 battery, CO_2 is served as working gas to provide and store energy sources by releasing and receiving electron during reduction and oxidation reaction process. This new energy device can not only capture CO_2 but also convert CO_2 to other pollution-free products, which can alleviate CO_2 concentration in the environment (Li et al., 2016; Qiao et al., 2017). Besides, the theoretical specific energy of Li–CO_2 battery can reach 1876 Wh Kg^{-1} based on the reaction of $4Li + 3CO_2 \rightarrow 2Li_2CO_3 + C$ (Liu et al., 2014; Zhang et al., 2015b; Li et al., 2016). Despite its huge potential, it still faces many difficulties. Firstly, it requires high energy to active the CO_2 due to the thermodynamic stability of CO_2, which results in the sluggish CO_2 reduction reaction (CO_2RR) kinetics (Pipes et al., 2019; Qiao et al., 2019). Secondly, the main discharge product Li_2CO_3 produced by the reaction is a wide-band gap insulating material, which shows a higher decomposition potential (>4.3 V vs. Li^+/Li) during charging (Garcia-Lastra et al., 2013; Ling et al., 2014; Liu et al., 2017). Therefore, this discharge product leads to a large overpotential, cycle instability, and poor rate performance, ultimately battery failure (Lim et al., 2013; Ling et al., 2014; Li et al., 2017; Xie et al., 2017; Yin et al., 2017).

In order to solve these problems, researchers have proven that good catalysts can promote the decomposition of Li_2CO_3 and improve the performance of Li–CO_2 batteries. Nanocarbon materials [carbon nanotubes (Zhang et al., 2015a), graphene (Zhang et al., 2015b), KB (Wang et al., 2017) etc.] and heteroatom-doped carbon materials (Qie et al., 2017), precious metals (Yang et al., 2017; Wang et al., 2018), transition metals (Zhang et al., 2018b, 2019) and their oxides (Zhang et al., 2018a; Lu et al., 2019), carbides (Hou et al., 2017; Zhou et al., 2018a) etc. are investigated. These catalysts can not only effectively reduce the decomposition potential (<4 V) of Li_2CO_3, promote the kinetics and thermodynamics of CO_2 reduction reaction (CO_2RR) and CO_2 evolution reaction (CO_2ER), but also improve the cycling stability of the battery (Qiao et al., 2017; Liu et al., 2019a), However, the rechargeability of Li–CO_2 battery is still far from the level of practical application because of low cycle performance, high charge potential and large overpotential (Hu et al., 2019; Liu et al., 2019a), and it is important to further design high efficient and low-cost catalysts (Liu et al., 2019a). Mn-based oxides are one of the promising catalysts because of their various crystal structures, high activity and low-cost prices (Chen et al., 2012; Zhang et al., 2015).

Because of its rich crystal structure, adjustable valence and unique MnO_6 octahedral effect, MnO_2 is widely used in the field of catalysis (Liu et al., 2018). However, the MnO_2 cathode will undergo severe structural degradation during the cycle, resulting in a decrease in cycle performance (Zhang et al., 2017). During the synthesis process, the tunnel structure of MnO_2 is inserted into cations (such as K^+, Ba^{2+}) to stabilize the structure between the guest ion and the host atom (Zhai et al., 2011; Yuan et al., 2015). In addition, the intercalation of cations can also enhance the diffusion of ions in the MnO_2 structure, thereby increasing the electronic conductivity to enhance its catalytic effect (Hao et al., 2019). Therefore, in this work, we synthesized K^+ doped MnO_2 nanowires networks with three-dimensional interconnections (3D KMO NWs) by a simple hydrothermal method. It should be noted that KMO nanowires with 3D interconnected structure can facilitate charge transfer and boost energy storage. As expected, the as-prepared 3D KMO NWs catalyst with interconnected network could promote the transfer of CO_2 and the decomposition of discharge products effectively (**Scheme 1**). Meanwhile, K^+ can effectively stabilize Mn-based materials, and the high content of K^+ can promote the octahedral effect of MnO_6 and the diffusion of ions, thereby enhancing the catalytic activity of main MnO_2 hosts for CO_2ER and CO_2RR. As a result, which exhibit an improved specific discharge capacity of 9043.0 mAh g^{-1} with decreased overpotential and improved cycling stability.

EXPERIMENTAL SECTION

Materials Preparation

3D KMO NWs were prepared by a simple hydrothermal method. Typically, 20 mmol $KMnO_4$ and 60 mmol urea were dissolved in 80 mL deionized water and stirred for 30 min. Afterwards, the obtained solution was transferred to a 100 mL Teflon-lined autoclave, then sealed and heated for 12 h at 120°C. Subsequently, 3D KMO NWs were collected after filtration and drying at 80°C for 12 h. In addition, two other samples were also prepared under different ration of $KMnO_4$ to urea.

Materials Characterizations

X-ray diffraction (XRD) patterns of as-prepared samples were investigated using a Bruker D8 X-ray diffractometer with a scanning rate of 5° min^{-1}. The microstructure morphologies were observed using scanning electron microscopy (SEM, JSM-7900F) and transmission electron microscopy (TEM, TECNAI G2 F20). N_2 adsorption/desorption isotherms were obtained by Novatouch LX2. The element analysis of the sample is tested by X-ray photoelectron spectroscopy (XPS, ESCALAB 250Xi). Raman spectra were recorded using a Renishaw in-Via confocal Raman spectrometer.

Electrochemical Measurements

To assess the energy storage properties, CR2032 coin-type battery was assembled on the condition of H_2O and O_2 lower than 0.01 ppm with lithium foil, GD/F Whatman glass fibers and 1 M LiTFSI in TEGDME organic solution as counter electrode, separators and electrolyte, respectively. To prepare an air electrode, 60 wt% of 3D KMO NWs, 30 wt% of KB and 10 wt% PVDF were mixed and made into slurry with NMP as solvent and cast on carbon paper. After drying at 80°C under vacuum, the electrodes were cut into disks with a diameter of 14 mm. Before testing, the as-assembled batteries were aged for 12 h in high-purity CO_2 atmosphere. The cyclic voltammetry (CV) test was performed on a CHI660E electrochemical workstation, the scanning range is 2.0–4.5 V and the scanning rate is 0.2 mV s^{-1}. Electrochemical impedance spectroscopy (EIS) curves were

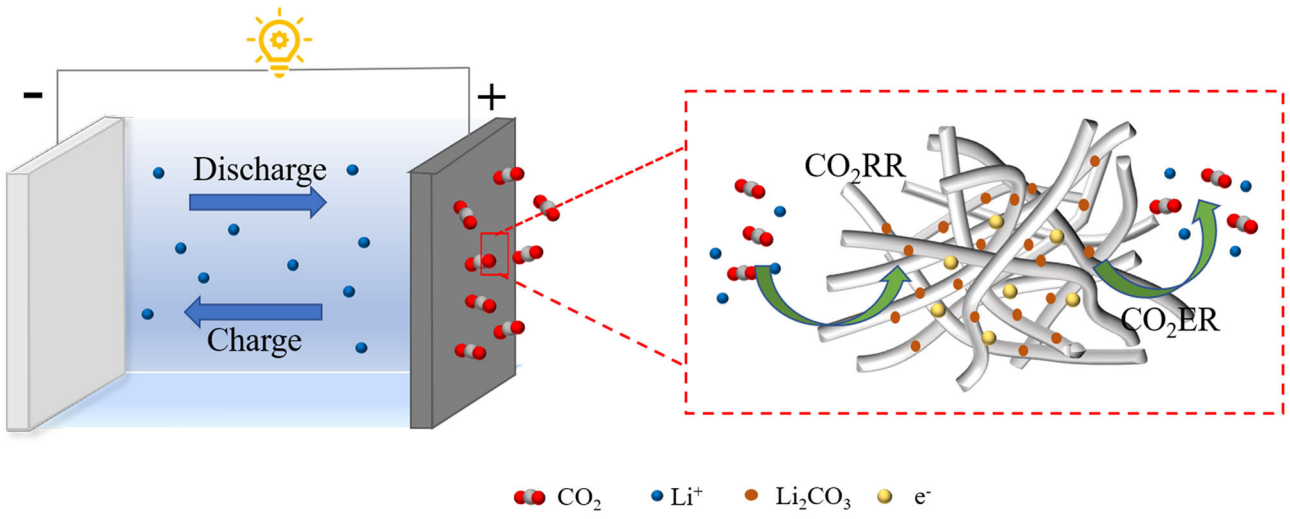

SCHEME 1 | Schematic illustration of the proposed catalytic mechanism based on the 3D KMO NWs cathode catalyst.

obtained in the frequency range of 0.01–100k Hz. Galvanostatic discharge and charge measurements were performed using a Shenzhen Neware BTS 3000 battery test system. For better comparison, bare electrode comprised of 90 wt% KB and 10 wt% PVDF was prepared in the same manner.

RESULTS AND DISCUSSION

Typically, $KMnO_4$ and urea solution were mixed with a specific molar ratio and afterwards underwent a facile hydrothermal process. During the hydrothermal process, urea is used to reduce $KMnO_4$ to MnO_2. As shown in **Figure 1a**, the XRD results of the products with different $KMnO_4$ and urea ratios show that the peak strength of MnO_2 gradually increases with the increase of urea concentration, and the prepared samples can be indexed as α-MnO_2 (PDF # 44-0141). This may be due to the intercalation of K^+ into MnO_2, which makes the peak strength of KMO lower than that of α-MnO_2, leading to the appearance of some peaks is not very obvious. Afterwards, the two samples were named as KMO and α-MnO_2, respectively. Through the inductively coupled plasma optical emission spectrometry (ICP-OES) analysis, the chemical composition of KMO, 3D KMO NWs and α-MnO_2 (the ratio of K and Mn) was determined, which were $K_{0.13}MnO_2$, $K_{0.18}MnO_2$, and $K_{0.08}MnO_2$, respectively. About 1.5 K^+ in per 8 Mn is embedded in the main channel of MnO_2. In theory, there is 2 K^+ in per 8 Mn, which shows that K^+ is approximately filled in the main channel of MnO_2 (Liu et al., 2019b). The morphologies and structures of as-prepared 3D KMO NWs were observed by scanning electron microscopy (SEM) and transmission electron microscopy (TEM). The SEM images in **Figure 1b** clearly presented a 3D interconnected networks comprised of considerable KMO nanowires with 10∼20 nm in diameter and several micrometers in length. It also can be seen from the result of EDX that K, Mn and O are evenly distributed in the sample. On the one hand, the as-prepared nanowires with high aspect ratios should account for high surface area, which contributed to shortening transfer paths and exposing more active sites for facilitate the reversible conversion of formed Li_2CO_3. On the other hand, the 1D nanowire structure could direct the electron transport axially owing to their inherent features, which lead to accelerate the reaction kinetics and boost the electrochemical performance. To make things better, apart from further promoting the charge transfer, the interconnected networks could improve the penetration of electrolyte and decrease transfer barriers (Mai et al., 2014). Through KMO (**Figure 1c**), the production of nanowires can still be seen, but there are still many particles that have not grown into nanowires clustered together, and the α-MnO_2 are nanorods (**Figure 1d**).

While in TEM images, as shown in **Figure 2a**, the 3D interconnected KMO networks obviously exhibited nanowires-like structure with interspaces, further enhancing the penetration of electrolyte and promoting electrochemical performance. The high-resolution TEM (HRTEM) images in **Figure 2b** show vast well-resolved lattice fringes, confirming the excellent crystallinity. The insets displayed typical lattice spacing of 0.346 nm and 0.309 nm, which corresponded to the (220) plane and (310) plane of α-MnO_2, respectively. Moreover, five diffraction rings could be observed through the selected area electron diffraction (SAED) pattern (**Figure 2c**), confirming a polycrystalline feature. Additionally, the diffraction rings could be well-indexed to (110), (200), (310), (321), and (521) planes of α-MnO_2, which corresponds to the results of XRD.

To further demonstrate the composition of as-prepared samples, X-ray photoelectron spectroscopy (XPS) was performed as well. As shown in **Supplementary Figure 1**, the XPS survey of 3D KMO NWs exhibited K, Mn, O and C peaks. As shown in **Figure 3A**, theses peaks at 292.3 eV and 295.2 eV can be contributed to K (Qin et al., 2019). From **Figure 3B**, O 1s has two peaks at 529.8 eV and 531.7 eV, which are represented as lattice oxygen and adsorbed oxygen (Lee et al., 2001). In addition, Mn^{3+}

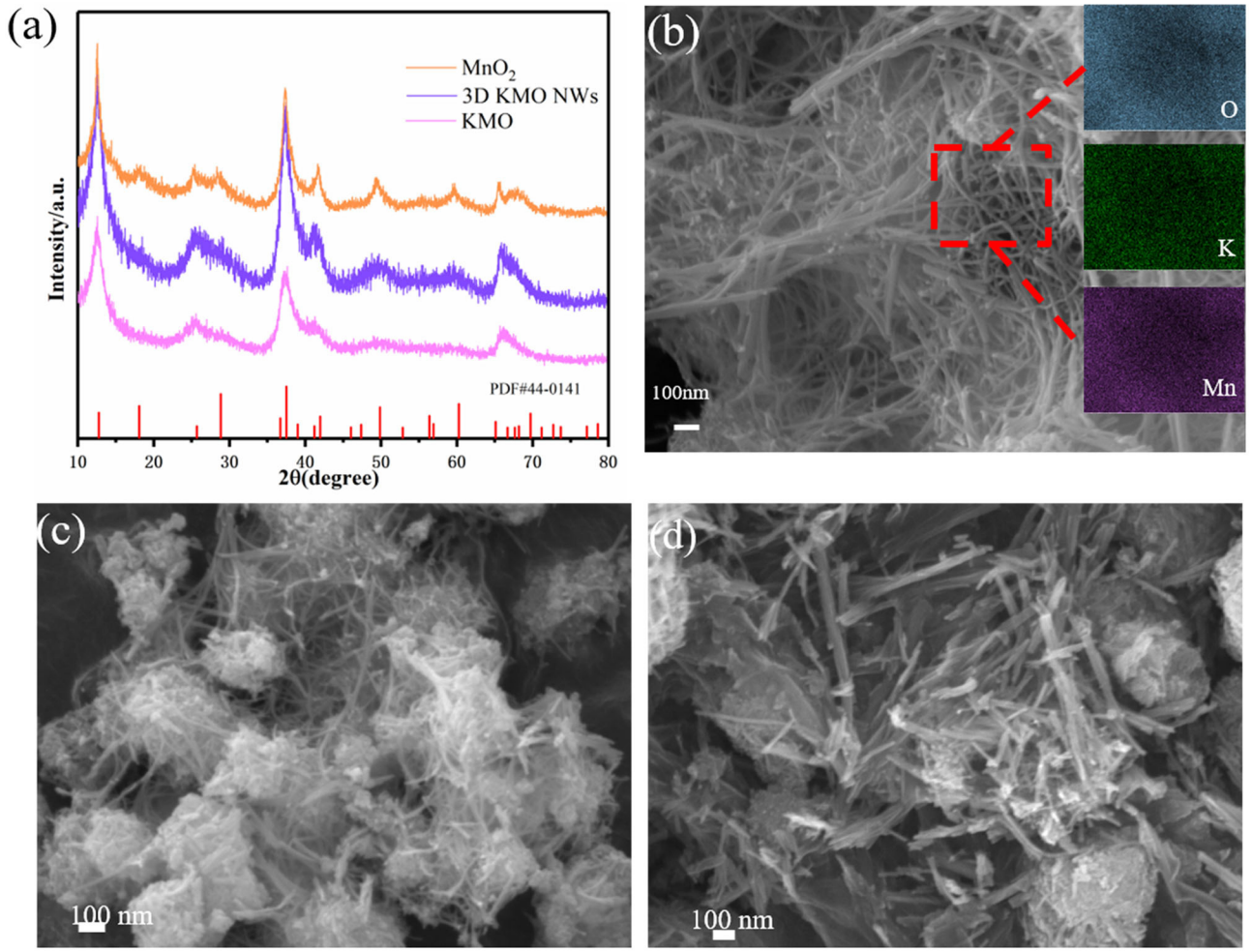

FIGURE 1 | (a) XRD pattern of 3D KMO NWs, KMO and MnO_2. **(b)** SEM images of 3D KMO NWs, and the inset of **(b)** is the element mapping of 3D KMO NWs. SEM images of KMO **(c)** and α-MnO_2 **(d)**, respectively.

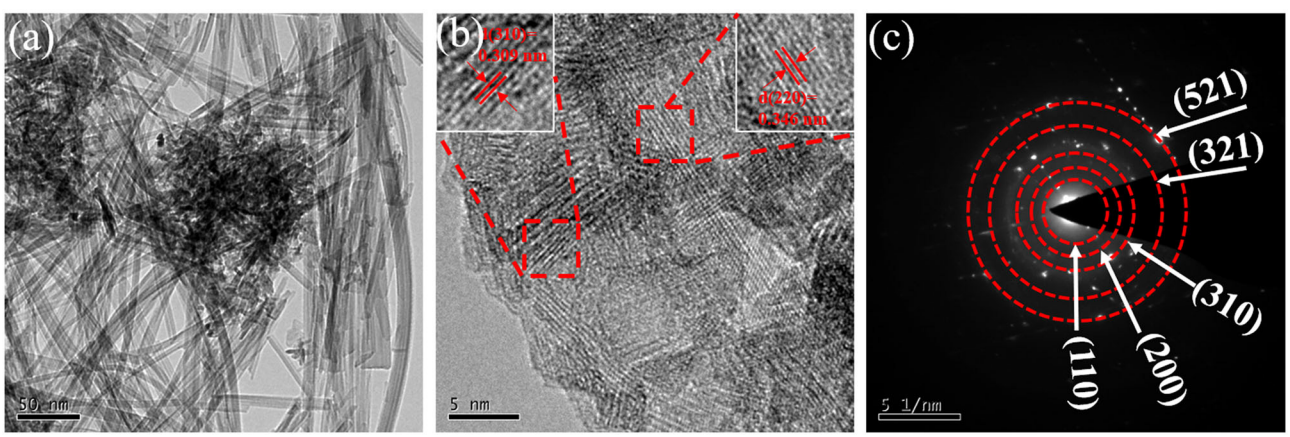

FIGURE 2 | (a) TEM images. **(b)** HRTEM images, and **(c)** SAED pattern of 3D KMO NWs.

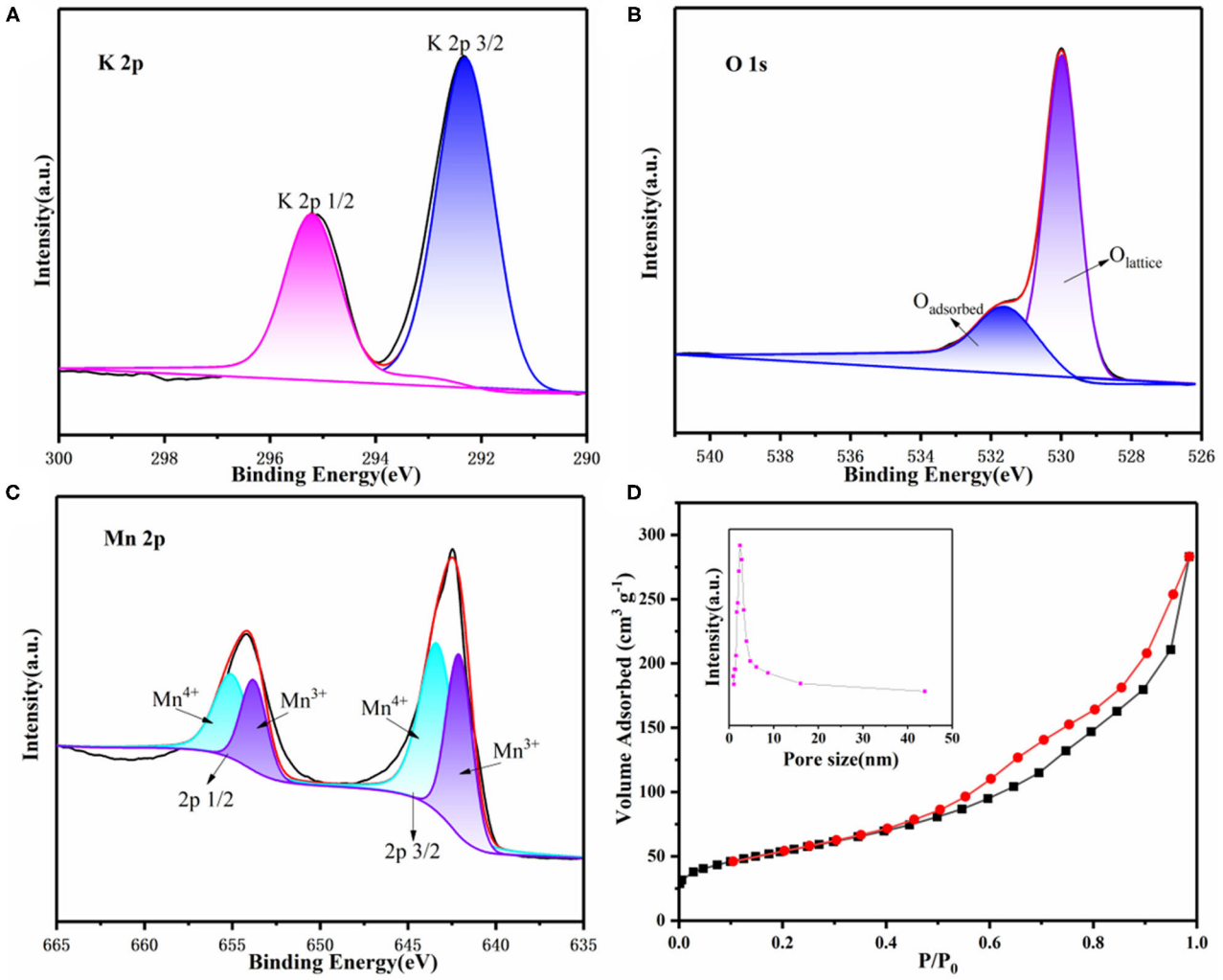

FIGURE 3 | XPS survey of **(A)** K 2p, **(B)** O 1s and **(C)** Mn 2p and **(D)** N_2 adsorption/desorption isotherm curves of 3D KMO NWs. The inset of (d) is the corresponding pore distribution of 3D KMO NWs.

and Mn^{4+} correspond to 642.3 eV and 643.5 eV, respectively (**Figure 3C**). The ratio of Mn^{4+} is higher than of Mn^{3+}, this means that the presence of K^+ could induce the charge-ordering of Mn^{4+} and Mn^{3+}, promoting the electron transport of α-MnO_2 (Liu et al., 2019b). N_2 adsorption/desorption isotherms was recorded to further show 3D KMO NWs porous feature. **Figure 3D** shows a typical Type IV isotherm of 3D KMO NWs. Calculated by Brunauer-Emmett-Teller (BET) method, the specific surface area of 3D KMO NWs is 193.1 $m^2\ g^{-1}$, therefore, the high specific surface area can also maximize the deposition of discharge products. The surface areas of KMO and α-MnO_2 are smaller than those of 3D KMO NWs, which are 174.3 $m^2\ g^{-1}$and 163.09 $m^2\ g^{-1}$ (**Supplementary Figure 2**), respectively. Additionally, the pore size distribution of 3D KMO NWs is about 2-10 nm (inset of **Figure 3D**), which demonstrates that its porous structure is mainly contributed by mesopores. These pores combined 3D porous networks could not only promote the transmission of CO_2 ions and electrolyte, but also provide enough space to deposit discharge products.

In order to study the influence of 3D KMO NWs on CO_2ER and CO_2RR, Li–CO_2 batteries were assembled and tested in a CO_2 atmosphere. Firstly, we tested the cyclic voltammogram (CV) to study the electrochemical activity of 3D KMO NWs in Li–CO_2 batteries with a voltage range of 2.0-4.5 V. Compared with KMO and α-MnO_2 (**Supplementary Figure 3b**), the oxidation peak area of 3D KMO NWs is larger than both of them, and it is also compared with commercial KB (**Supplementary Figure 3a**). The curve shows that the cathode peak area of 3D KMO NWs is larger than that of pure commercial KB, and the potential of the anode peak of 3D KMO NWs cathode is higher than that of pure commercial KB cathode. In addition, the anode current of 3D KMO NWs cathode is higher than that of KB. The results show that the 3D KMO NWs/KB composite material has enhanced activity for discharge

products (mainly about Li_2CO_3) decomposition. Secondly, to further prove the catalytic performance of 3D KMO NWs, the first cycle curves of Li–CO_2 batteries with the 3D KMO NWs/KB, KMO, α-MnO_2 and KB electrodes are shown in **Figure 4a**. The 3D KMO NWs/KB composite cathode exhibited the higher discharge capacity of 9,043 mAh g^{-1} (Liu et al., 2020). Even during the subsequent charging process, its terminal charging voltage is still lower than 4.3 V. The discharge capacities of KMO and α-MnO_2 are 6,460 mAh g^{-1} and 4,468 mAh g^{-1}, respectively, which are lower than 3D KMO NWs. In addition, the overpotential of the first cycle of 3D KMO NWs composite air cathode is ∼1.25 V (**Figure 4b**), which is lower than that of pure commercial KB (1.57 V), KMO (1.38 V) and α-MnO_2 (1.54 V). This indicates that α-MnO_2 and KMO with lower K^+ content have lower capacity in Li–CO_2 batteries and higher overpotential. On the contrary, 3D KMO NWs with high K^+ content shows

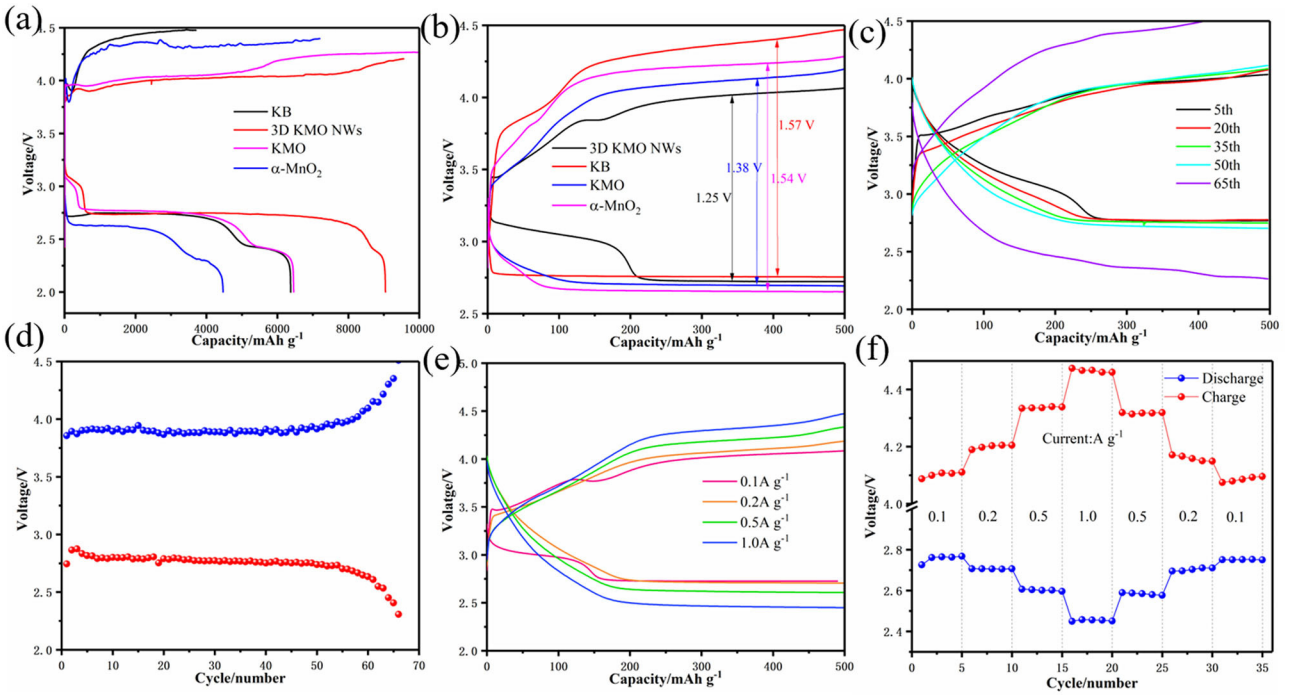

FIGURE 4 | (a) the full discharge-charge voltage curves at a current density of 100 mA g^{-1}, **(b)** the comparison of polarization at the first cycle, discharge-charge profiles of 3D KMO NWs, KMO, α-MnO_2 and KB, **(c)** the discharge-charge voltage curves within a limiting capacity of 500 mAh g^{-1} at a current density of 100 mA g^{-1} of 3D KMO NWs. **(d)** the relationship between the median voltage of 3D KMO NWs and the number of cycles. **(e)** Comparison of cycle curves of Li–CO_2 batteries with 3D KMO NWs at different current densities. **(f)** Rate performance of Li–CO_2 battery with 3D KMO NWs cathode at different current densities.

TABLE 1 | Comparison and summary of recent literatures on electrochemical performance of Li-CO_2 batteries with different cathodes.

Cathode	Current density (mA g^{-1})	Discharge capacity (mAh g^{-1})	Limited capacity (mAh g^{-1})	Cycle number	Overpotential(V)	References
Ketjen black	50	1,620	1,000	9	-	Zhang et al., 2015b
Cu_2O-Rd	100	6,235	500	50	1.9	Jena et al., 2020
Cu_2O-Cb	100	5,014	500	45	2.2	Jena et al., 2020
Cu_2O-Oh	100	3,314	500	45	2.4	Jena et al., 2020
Mn_3O_4	100	14,281	1,000	29	1.33	Liu et al., 2020
Ir/CNF	100	18,813	1,000	27	1.38	Wang et al., 2018
MnO@NC-G	50	25,021	1,000	15	0.88	Li et al., 2019
Ru/CNT	100	2,882	500	36	1.11	Chen et al., 2020
P-Mn_2O_3	50	9,434	1,000	50	1.40	Ma et al., 2018
CNT@RuO_2	100	-	500	30	1.51	Bie et al., 2019
α-MnO_2	100	4,468	500	31	1.54	This work
KMO	100	6,460	500	33	1.38	This work
3D KMO NWs	100	9,043	500	64	1.25	This work

good electrochemical performance. The increase in discharge capacity and the decrease in overpotential can be attributed to the large specific surface area and pore size of 3D KMO NWs, so that the discharge products can be deposited on the 3D KMO NWs to the greatest extent. On the other hand, high content of K^+ can enhance the diffusion of ions and electrons in the MnO_2 main channel, accelerate the transmission of ions and electrons, and provide more catalytic activity to promote the reaction kinetics of CO_2ER and CO_2RR.

The Li–CO_2 batteries with the 3D KMO NWs/KB composite materials were evaluate their cycle performance by galvanostatic discharge/charge test at a current density of 100 mA g^{-1} with a cut-off capacity of 500 mAh g^{-1}. Compared with others materials as cathodes, 3D KMO NWs/KB electrode showed about 64 cycles as shown in **Figure 4c**. As shown in **Supplementary Figure 4**, KMO can only cycle 33 times, while α-MnO_2 can only cycle 31 times (**Supplementary Figure 5**). And also evaluating the pure commercial KB can only cycle 13 times in the voltage range of 2.0–4.5 V, and after 13 cycles (**Supplementary Figure 6**), the charging potential has exceeded 4.5 V, indicating that pure commercial KB cannot effectively decompose the discharge product Li_2CO_3.It is exhibited a good cycle performance with 3D KMO NWs/KB electrode. Through the 3D KMO NWs discharge and charge median voltage (**Figure 4d**), it is found that the overpotential has been stable at about 1.15V before 55 cycles. After 55 cycles, the overpotential increased rapidly, which may be due to the complete oxidation of the Li anode, finally caused the battery to fail (Shui et al., 2013; Li et al., 2019). The overpotential of the median voltage is lower than the overpotential of the first cycle. This is mainly due to the fact that after one cycle of activation of the battery, electrolyte and gas will completely infiltrate, making the electrons transmission easier. The electrochemical results show that the high content of K^+ doping in the MnO_2 hosts can stabilize the structure of MnO_2,

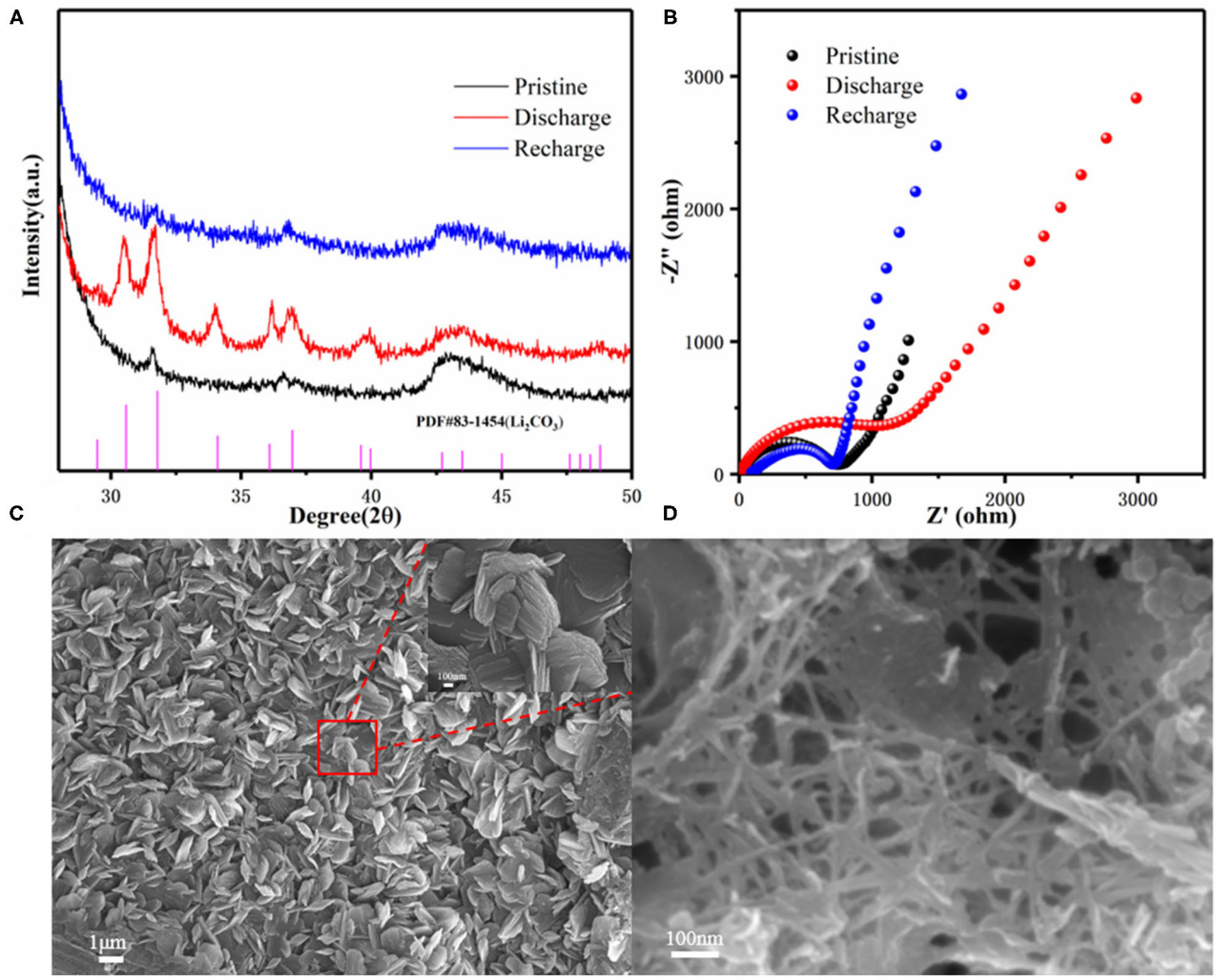

FIGURE 5 | Li–CO_2 battery **(A)** XRD of pristine, first discharge and first charge, **(B)** EIS of pristine first discharge and first charge, **(C)** SEM image after first discharge, inset is a partial enlarged image. **(D)** SEM image after first charging.

so that it has more stable cycle performance. Compared with the other two samples, the more K^+ embedded in the main MnO_2 hosts, the better the promotion of the octahedral effect of Mn-O, thereby enhancing the catalytic activity of the main MnO_2 hosts for CO_2ER and CO_2RR.

Through the discharge-charge curves under different current densities (**Figure 4e**), the discharge platform of the battery is 2.72 V at a current density of 0.1 A g^{-1}. After a cycle, the discharge platform of the battery has improved and stabilized at 2.76 V, while at different current densities of 0.2, 0.5, and 1.0 A g^{-1}, their discharge platforms are 2.71, 2.61, and 2.46 V, respectively. The discharge platform is higher than 2.4 V at a large current density of 1.0 A g^{-1}, indicating 3D KMO NWs has a good rate performance. In addition, the rate performance of Li–CO_2 battery with 3D KMO NWs/KB cathode was studied by discharging/charging five cycles with a cut-off capacity of 500 mAh g^{-1} under different current densities. As shown in **Figure 4f**, even at a higher current density (1.0 A g^{-1}), the charge potential of the 3D KMO NWs cathode is only 4.47 V, which is still lower than the set voltage range, and the discharge potential is also more than 2.4 V. In addition, after 30 cycles of different current densities, the charge potential returned to the previous 4.07 V, and the discharge potential remained the same as before. This shows that the Li–CO_2 battery with 3D KMO NWs cathode has good reversibility and stability after high current density. Therefore, 3D KMO NWs catalyst can not only improve the reaction kinetics of CO_2ER and CO_2RR, but also effectively improve the electrochemical performance of Li–CO_2 batteries (**Table 1**). The electrochemical reaction mechanism of Li–CO_2 battery is still unclear, but the research on the above-mentioned electrochemical performance partially proves that α-MnO_2 doped with different K^+ content has a greater influence

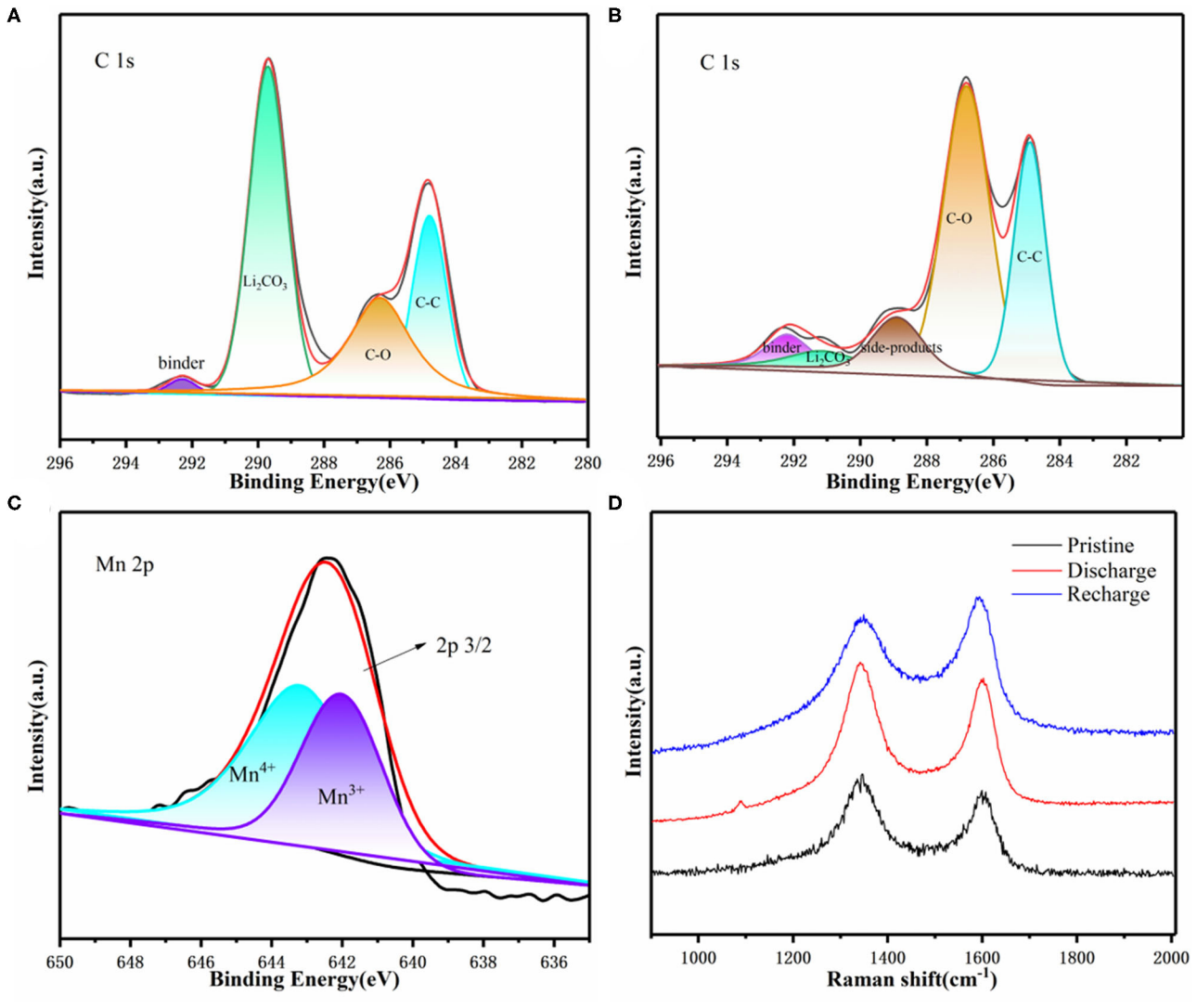

FIGURE 6 | Li–CO_2 battery **(A)** C1s XPS after first discharge, **(B)** C1s XPS after first charge, **(C)** XPS of Mn $2p_{3/2}$ after first charge. **(D)** Raman spectra of the pristine, first discharge and first charge.

on the electrochemical reaction of Li–CO_2. The high content of K^+ doping can not only effectively increase the ion and electron diffusion in the tunnel of the MnO_2 hosts, promote the octahedral effect of Mn-O, but also stabilize the structure of α-MnO_2, which can improve the catalytic activity of CO_2 and make it have more stable electrochemical performance.

To further understand the reversible reduction and evolution of CO_2 on the 3D KMO NWs cathode, we further characterized the formation and decomposition of discharge products in the electrochemical process through *ex-situ* XRD, EIS, XPS, and Raman. As shown in **Figure 5A**, there is no obvious XRD peak over 28° of 2θ displayed on the pristine 3D KMO NWs electrode except for the peak of carbon paper. The extra peaks in the XRD curve of the discharge electrode are all attributed to Li_2CO_3 (PDF#83-1454), and the disappearance of these peaks after the recharging process is attributed to the high reversibility of the efficient cathode catalyst. This is consistent with previous reports (Zhou et al., 2018b; Wang et al., 2019). **Figure 5B** shows the electrochemical impedance spectroscopy (EIS) spectra of the Li–CO_2 batteries with 3D KMO NWs cathode. Compared with electrode of different electrochemical states, due to the formation of insulating Li_2CO_3 during the discharge process, the EIS pattern displayed a significantly larger semicircle by the discharge product, which increased the interface and charge transfer impedance (Qie et al., 2017). The subsequent recharging process, interface impedance resistance recovered similar to the EIS spectrum of the pristine electrode, indicating that the Li_2CO_3 had been efficiently decomposed during the charging process. This is corresponded to the XRD results (Hu et al., 2020).

In order to further clarify the discharging/charging processes of Li–CO_2 battery. The 3D KMO NWs cathode after the discharging and charging processes were characterized by SEM. **Figure 5C** shows the discharging cathode, the thin plate-shaped discharge product Li_2CO_3 (≈300 nm) gradually deposited, aggregated and finally completely covered the electrode surface (Xing et al., 2018; Guo et al., 2019). After recharging, the discharge products disappear completely, and only 3D KMO NWs can be observed in **Figure 5D**. Therefore, it can be confirmed that the 3D interconnected 3D KMO NWs have good catalytic performance for the decomposition of Li_2CO_3.

We also used XPS analysis to explore related catalytic mechanisms (**Figures 6A–C**). Through the analysis of the C 1s spectrum of 3D KMO NWs, it was found that it corresponds to a high intensity Li_2CO_3 peak (289.8 eV) in the discharge state (**Figure 6A**). The peak almost disappeared during recharging, indicating that the 3D interconnected 3D KMO NWs nanowires have good catalytic performance for CO_2ER (**Figure 6C**) (Xing et al., 2018). In addition, being similar to the original 3D KMO NWs, the high-resolution spectrum of Mn $2p_{3/2}$ also showed two constant peaks at 642.3 eV and 643.5 eV, which corresponding to Mn^{3+} and Mn^{4+}, respectively, after recharging. The result shows that it is possible to suppress the Mn dissolution as the K^+ ions steadily intercalated into the tunnels of 3D KMO NWs and bonded with the Mn polyhedrons, enhancing its inherent stability (Fang et al., 2019; Liu et al., 2019b). Therefore, it shows that 3D KMO NWs has good stability during charging and discharging. Through Raman spectroscopy (**Figure 6D**), the two peaks at 1,350 and 1,580 cm^{-1} are represented as the D-band and G-band of C, respectively. It is also found that there is a Li_2CO_3 peak at 1,080 cm^{-1} during discharging, and the peak disappears after charging, which further reveals the formation and decomposition of Li_2CO_3 during discharging and charging. The above results show that the product produced by Li-CO_2 battery discharge is mainly Li_2CO_3, and Li_2CO_3 can be reversibly decomposed through the subsequent charging process.

CONCLUSIONS

In summary, a K^+ doped 3D KMO NWs catalyst for Li–CO_2 batteries was provided and prepared by a simple hydrothermal method. It can effectively improve the performance of Li–CO_2 batteries. This 3D network structure can promote Li^+ diffusion, CO_2 transfer and deposition/decomposition of Li_2CO_3. And the high content of K^+ can stabilize the Mn-based positive electrode to improve the cycle stability. Compared with the lower K^+ content of KMO and α-MnO_2, the prepared 3D KMO NWs with high content of K^+ have longer cycle life, lower overpotential and better rate performance, which is mainly due to the better morphology and high content of K^+ that improves the ion conductivity and stabilizes the structure of the MnO_2 hosts, thereby improving the catalytic performance of the MnO_2 hosts. In addition, *ex-situ* XRD, SEM, XPS, and Raman analysis showed that the discharge product Li_2CO_3 was almost completely decomposed after recharging. Therefore, this strategy of doping K^+ in MnO_2 catalyst provides a new path for the further design of Li-CO_2 battery.

DATA AVAILABILITY STATEMENT

The original contributions presented in the study are included in the article/**Supplementary Material**, further inquiries can be directed to the corresponding author.

AUTHOR CONTRIBUTIONS

ZT conducted the experiments and write the manuscript. MY and JL helped with experiments and data analysis. GZ and ZC explained the results. HZ, JD, and ZC supervised the research. All authors approved the submission of final manuscript.

FUNDING

This work was supported by the National Natural Science Foundation of China (No. 51874048), the Research Foundation of Education Bureau of Hunan Province (No. 19A003) and Scientific Research Fund of Changsha Science and Technology Bureau (No. kh2003021).

SUPPLEMENTARY MATERIAL

The Supplementary Material for this article can be found online at: https://www.frontiersin.org/articles/10.3389/fchem.2021.670612/full#supplementary-material

REFERENCES

Appel, A. M., Bercaw, J. E., Bocarsly, A. B., Dobbek, H., DuBois, D. L., Dupuis, M., et al. (2013). Frontiers, opportunities, and challenges in biochemical and chemical catalysis of CO_2 fixation. *Chem. Rev.* 113, 6621–6658. doi: 10.1021/cr300463y

Bie, S., Du, M., He, W., Zhang, H., Yu, Z., Liu, J., et al. (2019). Carbon nanotube@RuO_2 as a high performance catalyst for Li-CO_2 batteries. *ACS Appl. Mater. Interfaces* 11, 5146–5151. doi: 10.1021/acsami.8b20573

Chen, C. J., Yang, Y. J., Chen, C. H., Wei, D. H., Hu, S. F., and Liu, R. S. (2020). Improvement of lithium anode deterioration for ameliorating cyclabilities of non-aqueous Li-CO_2 batteries. *Nanoscale* 12, 8385–8396. doi: 10.1039/D0NR00971G

Chen, Z. W., Jiao, Z., Pan, D. Y., Li, Z., Wu, M. H., Shek, C. H., et al. (2012). Recent advances in manganese oxide nanocrystals: fabrication, characterization, and microstructure. *Chem. Rev.* 112, 3833–3855. doi: 10.1021/cr2004508

Chu, S., and Majumdar, A. (2012). Opportunities and challenges for a sustainable energy future. *Nature* 488, 294–303. doi: 10.1038/nature11475

De Bhowmick, G., Sarmah, A. K., and Sen, R. (2019). Zero-waste algal biorefinery for bioenergy and biochar: a green leap towards achieving energy and environmental sustainability. *Sci. Total Environ.* 650, 2467–2482. doi: 10.1016/j.scitotenv.2018.10.002

Fang, G., Zhu, C., Chen, M., Zhou, J., Tang, B., Cao, X., et al. (2019). Suppressing manganese dissolution in potassium manganate with rich oxygen defects engaged high-energy-density and durable aqueous zinc-ion battery. *Adv. Funct. Mater.* 29:1808375. doi: 10.1002/adfm.201808375

Garcia-Lastra, J. M., Myrdal, J. S. G., Christensen, R., Thygesen, K. S., and Vegge, T. (2013). DFT+U study of polaronic conduction in Li_2O_2 and Li_2CO_3: implications for Li–Air batteries. *J. Phys. Chem. C* 117, 5568–5577. doi: 10.1021/jp3107809

Guo, Z., Li, J., Qi, H., Sun, X., Li, H., Tamirat, A. G., et al. (2019). A Highly Reversible Long-Life Li-CO_2 battery with a RuP_2 -based catalytic cathode. *Small* 15:e1803246. doi: 10.1002/smll.201970155

Hao, Z., Shen, Z., Li, Y., Wang, H., Zheng, L., Wang, R., et al. (2019). The role of alkali metal in alpha-MnO_2 catalyzed ammonia-selective catalysis. *Angew. Chem. Int. Ed Engl.* 58, 6351–6356. doi: 10.1002/anie.201901771

Hou, Y., Wang, J., Liu, L., Liu, Y., Chou, S., Shi, D., et al. (2017). Mo_2C/CNT: an efficient catalyst for rechargeable Li-CO_2 batteries. *Adv. Funct. Mater.* 27:1700564. doi: 10.1002/adfm.201700564

Hu, A., Shu, C., Xu, C., Liang, R., Li, J., Zheng, R., et al. (2019). Design strategies toward catalytic materials and cathode structures for emerging Li–CO_2 batteries. *J. Mater. Chem. A.* 7, 21605–21633. doi: 10.1039/C9TA06506G

Hu, C. G., Gong, L. L., Xiao, Y., Yuan, Y. F., Bedford, N. M., Xia, Z. H., et al. (2020). High-Performance, long-life, rechargeable Li-CO_2 batteries based on a 3D holey graphene cathode implanted with single iron atoms. *Adv. Mater. Weinheim.* 32:1907436. doi: 10.1002/adma.201907436

Jang, J. G., Kim, G. M., Kim, H. J., and Lee, H. K. (2016). Review on recent advances in CO_2 utilization and sequestration technologies in cement-based materials. *Constr. Build. Mater.* 127, 762–773. doi: 10.1016/j.conbuildmat.2016.10.017

Jena, A., Hsieh, H. C., Thoka, S., Hu, S. F., Chang, H., and Liu, R. S. (2020). Curtailing the overpotential of Li-CO_2 batteries with shape-controlled Cu_2O as cathode: effect of illuminating the cathode. *ChemSusChem* 13, 2719–2725. doi: 10.1002/cssc.202000097

Khurram, A., He, M., and Gallant, B. M. (2018). Tailoring the discharge reaction in Li-CO_2 batteries through incorporation of CO_2 capture chemistry. *Joule* 2, 2649–2666. doi: 10.1016/j.joule.2018.09.002

Lee, Y. N., Lago, R. M., Fierro, J. L. G., Cortés, V., Sapiña, F., and Mart'inez, E. (2001). Surface properties and catalytic performance for ethane combustion of $La_{1\_x}K_xMnO_{3+\delta}$ perovskites. *Appl. Catal. A Gen.* 201, 17–24. doi: 10.1016/S0926-860X(00)00610-4

Li, C., Guo, Z., Yang, B., Liu, Y., Wang, Y., and Xia, Y. (2017). A rechargeable Li-CO_2 battery with a gel polymer electrolyte. *Angew. Chem. Int. Ed.* 56, 9126–9130. doi: 10.1002/anie.201705017

Li, S., Liu, Y., Zhou, J., Hong, S., Dong, Y., Wang, J., et al. (2019). Monodispersed MnO nanoparticles in graphene-an interconnected N-doped 3D carbon framework as a highly efficient gas cathode in Li–CO_2 batteries. *Energy Environ. Sci.* 12, 1046–1054. doi: 10.1039/C8EE03283A

Li, X., Yang, S., Feng, N., He, P., and Zhou, H. (2016). Progress in research on Li–CO_2 batteries: mechanism, catalyst and performance. *Chin. J. Catal.* 37, 1016–1024. doi: 10.1016/S1872-2067(15)61125-1

Lim, H. K., Lim, H. D., Park, K. Y., Seo, D. H., Gwon, H., Hong, J., et al. (2013). Toward a lithium-"air" battery: the effect of CO_2 on the chemistry of a lithium-oxygen cell. *J. Am. Chem. Soc.* 135, 9733–9742. doi: 10.1021/ja4016765

Ling, C., Zhang, R., Takechi, K., and Mizuno, F. (2014). Intrinsic barrier to electrochemically Decompose Li_2CO_3 and LiOH. *J. Phys. Chem. C* 118, 26591–26598. doi: 10.1021/jp5093306

Liu, B., Sun, Y., Liu, L., Chen, J., Yang, B., Xu, S., et al. (2019a). Recent advances in understanding Li–CO_2 electrochemistry. *Energy Environ. Sci.* 12, 887–922. doi: 10.1039/C8EE03417F

Liu, B., Sun, Y., Liu, L., Xu, S., and Yan, X. (2018). Advances in manganese-based oxides cathodic electrocatalysts for Li-Air batteries. *Adv. Funct. Mater.* 28:1704973. doi: 10.1002/adfm.201704973

Liu, G., Huang, H., Bi, R., Xiao, X., Ma, T., and Zhang, L. (2019b). K^+ pre-intercalated manganese dioxide with enhanced Zn^{2+} diffusion for high rate and durable aqueous zinc-ion batteries. *J. Mater. Chem. A.* 7, 20806–20812. doi: 10.1039/C9TA08049J

Liu, L. M., Zhang, L. B., Wang, K., Wu, H., Mao, H., Li, L., et al. (2020). Understanding the dual-phase synergy mechanism in Mn_2O_3-Mn_3O_4 catalyst for efficient Li-CO_2 batteries. *ACS Appl. Mater. Inter.* 12, 33846–33854. doi: 10.1021/acsami.0c09644

Liu, Y., Wang, R., Lyu, Y., Li, H., and Chen, L. (2014). Rechargeable Li/CO_2-O_2(2:1) battery and Li/CO_2 battery. *Energy Environ. Sci.* 7, 667–681. doi: 10.1039/c3ee43318h

Liu, Z., Zhang, Y., Jia, C., Wan, H., Peng, Z., Bi, Y., et al. (2017). Decomposing lithium carbonate with a mobile catalyst. *Nano Energy* 36, 390–397. doi: 10.1016/j.nanoen.2017.04.049

Lu, S., Shang, Y., Ma, S., Lu, Y., Liu, Q. C., and Li, Z. J. (2019). Porous NiO nanofibers as an efficient electrocatalyst towards long cycling life rechargeable Li–CO_2 batteries. *Electrochim. Acta* 319, 958–965. doi: 10.1016/j.electacta.2019.07.062

Ma, W., Lu, S., Lei, X., Liu, X., and Ding, Y. (2018). Porous Mn_2O_3 cathode for highly durable Li–CO_2 batteries. *J. Mater. Chem. A.* 6, 20829–20835. doi: 10.1039/C8TA06143B

Mai, L., Tian, X., Xu, X., Chang, L., and Xu, L. (2014). Nanowire electrodes for electrochemical energy storage devices. *Chem. Rev.* 114, 11828–11862. doi: 10.1021/cr500177a

Nguyen, T. N., and Dinh, C.-T. (2020). Gas diffusion electrode design for electrochemical carbon dioxide reduction. *Chem. Soc. Rev.* 49, 7488–7504. doi: 10.1039/D0CS00230E

Pipes, R., He, J., Bhargav, A., and Manthiram, A. (2019). Efficient Li–CO_2 batteries with molybdenum disulfide nanosheets on carbon nanotubes as a catalyst. *ACS Appl. Energy Mater.* 2, 8685–8694. doi: 10.1021/acsaem.9b01653

Qiao, Y., Xu, S., Liu, Y., Dai, J., Xie, H., Yao, Y., et al. (2019). Transient, *in situ* synthesis of ultrafine ruthenium nanoparticles for a high-rate Li–CO_2 battery. *Energy Environ. Sci.* 12, 1100–1107. doi: 10.1039/C8EE03506G

Qiao, Y., Yi, J., Wu, S., Liu, Y., Yang, S., He, P., et al. (2017). Li-CO_2 electrochemistry: a new strategy for CO_2 fixation and energy storage. *Joule* 1, 359–370. doi: 10.1016/j.joule.2017.07.001

Qie, L., Lin, Y., Connell, J. W., Xu, J., and Dai, L. (2017). Highly rechargeable lithium-CO_2 batteries with a boron- and nitrogen-codoped holey-graphene cathode. *Angew. Chem. Int. Ed.* 56, 6970–6974. doi: 10.1002/anie.201701826

Qin, L., Lei, Y., Wang, H. W., Dong, J. H., Wu, Y. Y., Zhai, D. Y., et al. (2019). Capillary encapsulation of metallic potassium in aligned carbon nanotubes for use as stable potassium metal anodes. *Adv. Energy Mater.* 9:1901427. doi: 10.1002/aenm.201901427

Sanz-Perez, E. S., Murdock, C. R., Didas, S. A., and Jones, C. W. (2016). Direct capture of CO_2 from ambient air. *Chem. Rev.* 116, 11840–11876. doi: 10.1021/acs.chemrev.6b00173

Shui, J. L., Okasinski, J. S., Kenesei, P., Dobbs, H. A., Zhao, D., Almer, J. D., et al. (2013). Reversibility of anodic lithium in rechargeable lithium-oxygen batteries. *Nat. Commun.* 4:3255. doi: 10.1038/ncomms3255

Wang, C., Zhang, Q., Zhang, X., Wang, X. G., Xie, Z., and Zhou, Z. (2018). Fabricating Ir/C nanofiber networks as free-standing air cathodes for rechargeable Li-CO_2 batteries. *Small* 14:e1800641. doi: 10.1002/smll.201800641

Wang, H., Xie, K., You, Y., Hou, Q., Zhang, K., Li, N., et al. (2019). Realizing interfacial electronic interaction within ZnS quantum dots/N-rGO heterostructures for efficient Li–CO_2 batteries. *Adv. Energy Mater.* 9:1901806. doi: 10.1002/aenm.201901806

Wang, X.-G., Wang, C., Xie, Z., Zhang, X., Chen, Y., Wu, D., et al. (2017). Improving electrochemical performances of rechargeable Li–CO_2 batteries with an electrolyte redox mediator. *ChemElectroChem* 4, 2145–2149. doi: 10.1002/celc.201700539

Xie, Z., Zhang, X., Zhang, Z., and Zhou, Z. (2017). Metal-CO_2 batteries on the road: CO_2 from contamination gas to energy source. *Adv. Mater.* 29:1605891. doi: 10.1002/adma.201605891

Xing, Y., Yang, Y., Li, D., Luo, M., Chen, N., Ye, Y., et al. (2018). Crumpled Ir nanosheets fully covered on porous carbon nanofibers for long-life rechargeable lithium-CO_2 batteries. *Adv. Mater.* 30:e1803124. doi: 10.1002/adma.201803124

Yang, S., Qiao, Y., He, P., Liu, Y., Cheng, Z., and Zhu, J.-J., et al. (2017). A reversible lithium–CO_2 battery with Ru nanoparticles as a cathode catalyst. *Energy Environ. Sci.* 10, 972–978. doi: 10.1039/C6EE03770D

Yin, W., Grimaud, A., Lepoivre, F., Yang, C., and Tarascon, J. M. (2017). Chemical vs electrochemical formation of Li_2CO_3 as a discharge product in Li-O_2/CO_2 batteries by controlling the superoxide intermediate. *J. Phys. Chem. Lett.* 8, 214–222. doi: 10.1021/acs.jpclett.6b02610

Yuan, Y., Nie, A., Odegard, G. M., Xu, R., Zhou, D., Santhanagopalan, S., et al. (2015). Asynchronous crystal cell expansion during lithiation of K(+)-stabilized alpha-MnO_2. *Nano Lett.* 15, 2998–3007. doi: 10.1021/nl5048913

Zhai, D., Li, B., Xu, C., Du, H., He, Y., Wei, C., et al. (2011). A study on charge storage mechanism of α-MnO_2 by occupying tunnels with metal cations (Ba^{2+}, K^+). *J. Power Sources* 196, 7860–7867. doi: 10.1016/j.jpowsour.2011.05.015

Zhang, K., Han, X. P., Hu, Z., Zhang, X. L., Tao, Z. L., and Chen, J. (2015). Nanostructured Mn-based oxides for electrochemical energy storage and conversion. *Chem. Soc. Rev.* 44, 699–728. doi: 10.1039/C4CS00218K

Zhang, N., Cheng, F., Liu, J., Wang, L., Long, X., Liu, X., et al. (2017). Rechargeable aqueous zinc-manganese dioxide batteries with high energy and power densities. *Nat. Commun.* 8:405. doi: 10.1038/s41467-017-00467-x

Zhang, X., Wang, C., Li, H., Wang, X.-G., Chen, Y.-N., Xie, Z., et al. (2018a). High performance Li–CO_2 batteries with NiO–CNT cathodes. *J. Mater. Chem. A.* 6, 2792–2796. doi: 10.1039/C7TA11015D

Zhang, X., Zhang, Q., Zhang, Z., Chen, Y., Xie, Z., Wei, J., et al. (2015a). Rechargeable Li-CO_2 batteries with carbon nanotubes as air cathodes. *Chem. Commun.* 51, 14636–14639. doi: 10.1039/C5CC05767A

Zhang, Z., Wang, X. G., Zhang, X., Xie, Z., Chen, Y. N., Ma, L., et al. (2018b). Verifying the rechargeability of Li-CO_2 batteries on working cathodes of ni nanoparticles highly dispersed on N-doped graphene. *Adv. Sci.* 5:1700567. doi: 10.1002/advs.201700567

Zhang, Z., Yang, C., Wu, S., Wang, A., Zhao, L., Zhai, D., et al. (2019). exploiting synergistic effect by integrating ruthenium-copper nanoparticles highly Co-dispersed on graphene as efficient air cathodes for Li-CO_2 batteries. *Adv. Energy Mater.* 9:1802805. doi: 10.1002/aenm.201802805

Zhang, Z., Zhang, Q., Chen, Y., Bao, J., Zhou, X., Xie, Z., et al. (2015b). The first introduction of graphene to rechargeable Li-CO_2 batteries. *Angew. Chem., Int. Ed.* 54, 6550–6553. doi: 10.1002/anie.201501214

Zhou, J., Li, X., Yang, C., Li, Y., Guo, K., Cheng, J., et al. (2018a). A quasi-solid-state flexible fiber-shaped Li-CO2 battery with low overpotential and high energy efficiency. *Adv Mater.* 31:e1804439. doi: 10.1002/adma.201804439

Zhou, J., Li, X., Yang, C., Li, Y., Guo, K., Cheng, J., et al. (2018b). A quasi-solid-state flexible fiber-shaped Li-CO_2 battery with low overpotential and high energy efficiency. *Adv. Mater.* 31:e1804439.

Conflict of Interest: The authors declare that the research was conducted in the absence of any commercial or financial relationships that could be construed as a potential conflict of interest.